Conf-9209200--6

PNL-SA--20885

DE93 001514

ION-BEAM MODIFICATION OF $Gd_2Ti_2O_7$

W. J. Weber
N. J. Hess

September 1992

Presented at the
8th International Conference
on Ion Beam Modification
of Materials
September 7-11, 1992
Heidelberg, Germany

Work supported by
the U.S. Department of Energy
under Contract DE-AC06-76RLO 1830

Pacific Northwest Laboratory
Richland, Washington 99352

MASTER

ION-BEAM MODIFICATION OF $Gd_2Ti_2O_7$

W. J. WEBER and N. J. HESS

Pacific Northwest Laboratory, P.O. Box 999, Richland, Washington 99352 USA

Irradiation of $Gd_2Ti_2O_7$ with 3 MeV Ar^+ ions results in expansion of the unit-cell volume from defect accumulation as well as irradiation-induced amorphization. The damage cross-section for amorphization determined from X-ray diffraction analysis is 0.023 nm^2. Transmission electron microscopy and electron diffraction have confirmed the irradiation-induced amorphous character at high fluences. Raman spectroscopy indicates a decrease in scattered intensity and an increase in linewidth with fluence for the principal vibrational modes, consistent with increasing irradiation-induced disorder. The wavenumber of the most intense Raman peak at ~310 cm^{-1} (attributed to the O-Gd-O bending mode) decreases with fluence, indicating a change in bond angle. The increase in the wavenumber of the Raman peak at ~515 cm^{-1} (attributed to the Gd-O stretching mode) with fluence suggests a decrease in bond length. At intermediate fluences, a forbidden peak at 765 cm^{-1} becomes slightly activated by irradiation-induced disorder on the cation sites.

I. Introduction

Irradiation-induced amorphization is perhaps the most extreme form of ion-beam modification. This phenomenon is of interest because of its consequences for property changes as well as for its contribution to the fundamental understanding of structural stability in crystalline ceramics. The structural stability of natural minerals to self-radiation damage from trace uranium and thorium decay is also of interest to mineralogists, and the structural stability of ceramic materials in high-radiation environments is an important aspect of many nuclear-energy-related technologies. Gadolinium titanate, $Gd_2Ti_2O_7$, is related to the pyrochlore [1,2] class of metamict minerals and also has been identified as a potential host phase for long-lived actinides in nuclear wastes forms [3]. Previous studies of related natural minerals [1,2], a glass-ceramic waste form [3], and an actinide-doped synthetic phase [4,5] have shown that self-radiation damage from alpha decay in this and related titanate structures results in radiation-induced amorphization. The objective of the present study was to investigate and characterize the effects of 3 MeV Ar^+ irradiation on the structure of $Gd_2Ti_2O_7$. Some preliminary results have been reported previously [6].

2. Experimental procedures

2.1. Specimen preparation

Starting material for specimen preparation consisted of analytical reagent-grade gadolinium nitrate and isopropyl titanate. A stoichiometric mixture was wet milled in ethyl alcohol in an agate disk mill, air dried, and then heated at 725°C for 2 h to calcine the powder. The oxide precursor powder was mechanically ground to <45 μm particle size, pressed into disks at

138 MPa, and fired in air at 1400°C for 46 h. After sintering, X-ray diffraction analysis confirmed the cubic (*Fd3m, Z=8*) crystal structure for $Gd_2Ti_2O_7$. Powder specimens with an average particle size of ~2 μm were prepared for irradiation by fine grinding. Techniques discussed previously [7-10], which utilize a very dilute rubber cement solution, were used to prepare monolayers of these fine particles (~1 mg/cm^2) on aluminum plates for irradiation.

2.2. Irradiation conditions

The 3 MeV Ar^+ irradiations, utilizing the Dynamitron accelerator facility at Argonne National Laboratory, were carried out on monolayers of $Gd_2Ti_2O_7$ particles supported on vertical aluminum plates. The calculated range of the 3 MeV Ar^+, using the TRIM-90 program [11], is 1.14 μm (straggling of 0.19 μm). The displacements generated as a function of depth, based on TRIM-90 calculations and an assumed displacement energy of 25 eV, are shown in fig. 1. Since the calculated range of damage is less than the average particle size (~2 μm), material beyond the damage range will be initially unaffected by the displacement processes; however, defect transport into these regions may occur. The specimens were irradiated to fluences ranging from 0.5 to 300 ions/nm^2 (0.04 to 25 dpa), using an ion beam current of up to 6 μA scanned over a specimen area of 1.8 cm^2.

2.3. Measurement techniques

The changes in unit-cell parameters were determined to within ± 0.02% from X-ray diffraction (XRD) data obtained using a diffractometer system employing Cu Kα radiation. For these Ar^+-irradiated specimens, the entire

thickness of the monolayer was measured along with the aluminum support plate, which served as an external standard.

Transmission electron microscopy of several irradiated powders (after XRD analysis) was carried out by scrapping powder from the aluminum holder, suspending the irradiated powders in methanol, and collecting the powders on collodion-carbon substrates. The specimens were examined at 120 kV in a Philips EM400T electron microscope. Analytical electron microscopy, with the scanning transmission mode, was used to verify the chemical composition of the particles examined.

Raman spectra of unirradiated and irradiated powders were collected using an oblique (120°) incident beam angle and a 90° collection geometry to minimize scattering from the aluminum substrate. Raman spectra were obtained using a 200 mW laser excitation (488.0 nm) focused to a 50 μm spot size. The scattered light was collected by an aluminum elliptical mirror and focused on to the entrance slit of a triplespectrometer. Signals were measured by means of a liquid-nitrogen cooled charged-coupled detector. The depth probed by the 488.0 nm radiation is not known, but does not extend beyond the peak damage region.

3. Results and discussion

Both the relative XRD and Raman intensities decrease exponentially with cumulative ion fluence, as shown in fig. 2. The Raman intensity decreases more rapidly than the XRD intensity, which does not fall to zero because of the residual crystallinity that remains in regions of the particles that are beyond the Ar^+ range. The more rapid decrease in the Raman intensity may reflect a higher disordering/damage rate in the region probed by the laser.

The observed decreases in relative intensity, I/I_o, as a function of ion fluence, F, follow the expression:

$$I/I_o = (1-C)\ \exp(-DF) + C \qquad (1)$$

where D (a qualitative damage cross-section for amorphization) is related to the volume amorphized per incident ion and C is the average fraction of residual crystallinity due to material beyond the Ar^+ range. A nonlinear regression fit of eq. (1) to the XRD data yields values for D and C of 0.023 nm^2 and 16.6%, respectively. The damage cross section determined from the Raman data is 0.19 nm^2, with C=0 (Raman does not probe regions containing residual crystalllinity). The XRD damage cross section is small relative to the damage cross-sections (determined by similar techniques) for a number of readily amorphized ceramic oxides [7-10], in agreement with observations of Cm-doped specimens [5]. Although the relative change in XRD intensity might be assumed to be directly proportional to the fraction of crystalline phase remaining, the large uncertainty (±10-20%) associated with powder XRD intensity measurements, the complex dependence of I/I_o on crystalline disorder, and perturbations due to the effects of internal strain restrict any quantitative interpretation in terms of the crystalline fraction.

The change in unit-cell volume, $\Delta V_{uc}/V_o$, of $Gd_2Ti_2O_7$ as a function of ion fluence is shown in fig. 3. The observed unit-cell volume expansion follows the characteristic exponential behavior based on defect accumulation and given by the expression [12]:

$$\Delta V_{uc}/V_o = A\ [1 - \exp(-BF)] \qquad (2)$$

where A is the relative unit-cell volume change at saturation and B is related to the rate constant (per unit fluence) for simultaneous annealing of Frenkel defects during irradiation. Nonlinear regression analysis yields values of 1.47% and 0.046 nm^2 for A and B, respectively. The high-fluence data in fig. 3 suggests that the residual crystalline material (beyond the Ar^+ range) that is giving rise to the residual XRD pattern may have undergone some expansion due to the transport or migration of irradiation-induced defects into these regions from the peak damage region (fig. 1). These residual crystalline regions may eventually become amorphous if the defect concentrations become high enough to induce amorphization.

As shown in fig. 4, fully amorphous regions were observed by TEM, as well as confirmed by electron diffraction analysis, at a fluence of 150 ions/nm^2 for $Gd_2Ti_2O_7$. The amorphous powders, however, were very susceptible to recrystallization from beam heating. At lower fluences, the microstructure consisted of a dense concentration of small defects (2.5 to 5.0 nm diameter) observable by strain contrast imaging, similar to behavior observed in Cm-doped specimens of this material [5]. The defects are assumed to be highly-damaged regions (disordered or amorphous) from the subcascades (or overlap of subcascades) produced by the Ar^+. High-resolution imaging, which was almost impossible in these specimens, revealed several regions of ~2 nm diameter that lacked periodicity and may be associated with amorphous regions.

In addition to the decrease in scattered Raman intensity (fig. 2), analysis of the Raman spectra indicates a significant increase in linewidth with fluence for the principal vibrational modes of this structure, consistent with increasing irradiation-induced disorder. The increase in linewidth of the 310 cm^{-1} mode is shown in fig. 5. The wavenumber of the most intense

Raman peak at 310 cm^{-1}, which has been attributed to the O-Gd-O bending mode [13], decreases slightly with fluence, as also shown in fig. 5, indicating a change in O-Gd-O bond angle. The linewidth and wavenumber exhibit exponential dependencies on ion fluence with rate constants of 0.051 nm^{-1} and 0.089 nm^{-1}, respectively, similar to that determined for the unit-cell expansion. The wavenumber of the Raman peak at 515 cm^{-1}, which has been attributed to the Gd-O stretching mode [13], increases slightly with ion fluence (data not shown) indicating a change in this bond length. A symmetry forbidden peak at 765 cm^{-1} (attributed to disorder on the cation lattice [13]) that is not present in the unirradiated powders becomes activated under irradiation, presumably as a result of irradiation-induced cation disorder. The intensity of this forbidden peak increases slightly at intermediate fluences and then decreases.

The rapid decrease in intensity of the Raman-active modes (fig. 2) in this structure indicates a significant distortion of the bonds giving rise to the observed vibrational modes, similar to behavior observed in extended X-ray absorption fine structure (EXAFS) and X-ray absorption near-edge structure (XANES) studies of radiation-induced amorphization in related materials [14-16]. The observed shift of the Raman vibrational modes with fluence in $Gd_2Ti_2O_7$ is likewise similar to the shift in Raman modes observed in crystalline multicomponent oxides subjected to high hydrostatic pressure [17]; high-pressure XRD studies have correlated the reported shifts to higher frequencies at high pressure to decreases in bond lengths or changes in bond angles [18]. Consequently, the increase of the vibrational frequency of the 515 cm^{-1} mode in $Gd_2Ti_2O_7$ is most probably associated with a decrease in the Gd-O bond lengths with fluence, which is consistent with the decrease in cation-oxygen bond lengths measured by EXAFS in a related titanate as a result

of radiation-induced amorphization [15]. The interpretation of the Raman results are consistent with results from detailed EXAFS and XANES studies of related materials [14-16] that indicate that radiation-induced amorphization reduces the average coordination number of the metal-oxygen sites, slightly decreases the metal-oxygen bond lengths within the nearest-neighbor coordination polyhedra, and destroys the atomic periodicity beyond the first coordination sphere. These initial Raman measurements are encouraging, and future studies have been proposed to further utilize Raman spectroscopy as a probe of radiation damage in these and other materials.

Acknowledgments

The authors would like to thank Prof. L. Cartz and Prof. F. G. Karioris (Marquette University) for performing the Ar^+ irradiations, which were carried out utilizing the Dynamitron Accelerator Facility at Argonne National Laboratory. This research was supported by the U. S. Department of Energy, Office of Basic Energy Sciences under Contract DE-AC06-76RLO 1830.

References

[1] G. R. Lumpkin and R. C. Ewing, Phys. Chem. Minerals 16 (1988) 2.

[2] R. C. Ewing and R. F. Haaker, Nucl. Chem. Waste Management 1 (1980) 51.

[3] R. P. Turcotte, J. W. Wald, F. P. Roberts, J. M. Rusin, and W. Lutze, J. Am. Ceram. Soc. 65 (1982) 589.

[4] W. J. Weber, J. W. Wald, and Hj. Matzke, Mater. Lett. 3 (1985) 173.

[5] W. J. Weber, J. W. Wald, and Hj. Matzke, J. Nucl. Mater. 138 (1986) 196.

[6] W. J. Weber, N. J. Hess, and G. D. Maupin, Nucl. Inst. and Meth. B65 (1992) 102.

[7] L. Cartz, F. G. Karioris and R. A. Fournelle, Radiat. Eff. 54 (1981) 57.

[8] F. G. Karioris, K. A. Gowda, L. Cartz and J. C. Labbe, J. Nucl. Mater. 108 & 109 (1982) 748.

[9] F. G. Karioris, K. Ramasami, K. A. Gowda and L. Cartz, Phil. Mag. A 52 (1985) 525.

[10] E. R. Vance, L. Cartz and F. G. Karioris, J. Mater. Sci. 19 (1984) 2943.

[11] J. F. Ziegler, J. P. Biersack, and U. Littmark, The Stopping and Range of Ions in Solids (Pergamon Press, New York, 1985).

[12] W. J. Weber, R. K. Eby, and R. C. Ewing, J. Mater. Res. (1991) 1334.

[13] M. Oueslati, M. Balkanski, P. K. Moon, and H. L. Tuller, in: Solid State Ionics, Mat. Res. Soc. Symp. Proc. Vol 135, eds. G. Nazri, R. A. Huggins, and D. F. Shriver (Materials Research Society, Pittsburgh, 1989) p. 199.

[14] R. C. Ewing, B. C. Chakoumakos, G. R. Lumpkin, T. Murakami, R. B. Greegor, and F. W. Lytle, Nucl. Instr. and Meth. B32 (1988) 487.

[15] R. B. Greegor, F. W. Lytle, R. J. Livak, and F. W. Clinard, Jr., J. Nucl. Mater. 152 (1988) 270.

[16] R. B. Greegor, F. W. Lytle, G. W. Arnold, and R. C. Ewing, J. Non-Cryst. Solids 122 (1990) 121.

[17] R. M. Hazen and L. W. Finger, Amer. Mineral. 63 (1978) 297.

[18] N. L. Ross, M. Akaogi, A. Navrosky, J-I. Susaki, and P. McMillan, J. Geophys. Res. 92 (1986) 4685.

Figure Captions

Fig. 1. Calculated distribution of displacements for 3 MeV incident Ar^+ using TRIM-90 code [11].

Fig. 2. Relative XRD and Raman intensities of 3 MeV Ar^+ irradiated $Gd_2Ti_2O_7$ as functions of ion fluence.

Fig. 3. Unit-cell volume expansion, $\Delta V_{uc}/V_o$, of 3 MeV Ar^+ irradiated $Gd_2Ti_2O_7$ as a function of ion fluence.

Fig. 4. TEM image and electron diffraction pattern of $Gd_2Ti_2O_7$ showing amorphization induced by 3 MeV Ar^+ irradiation after a fluence of 150 ions/nm^2.

Fig. 5. Change in frequency and linewidth of Raman peak at ~310 cm^{-1} in $Gd_2Ti_2O_7$ as a function of ion fluence.

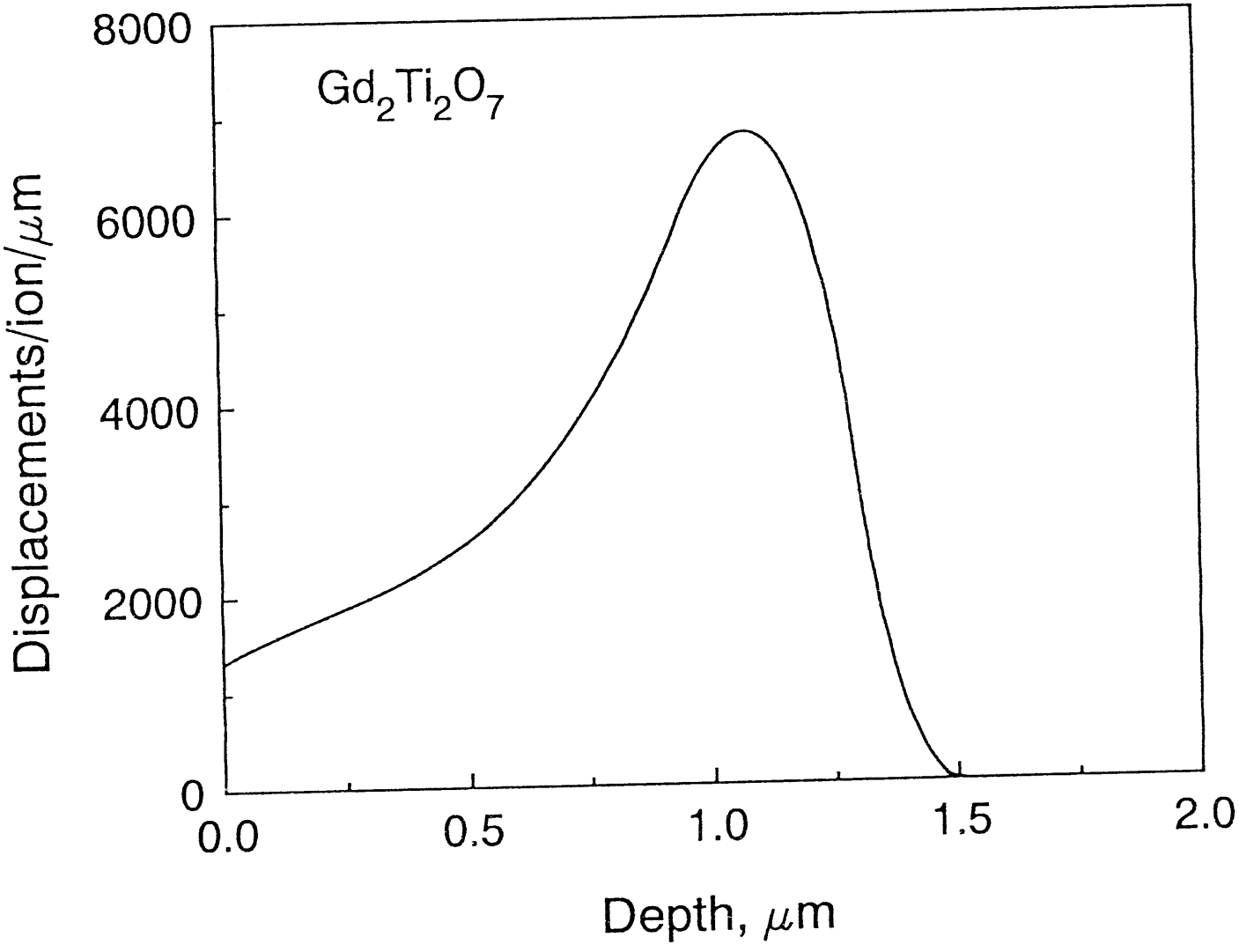
8000
6000
4000
2000
0
$Gd_2Ti_2O_7$
Displacements/ion/μm
0.0
0.5
1.0
1.5
2.0
Depth, μm

Fig. 1

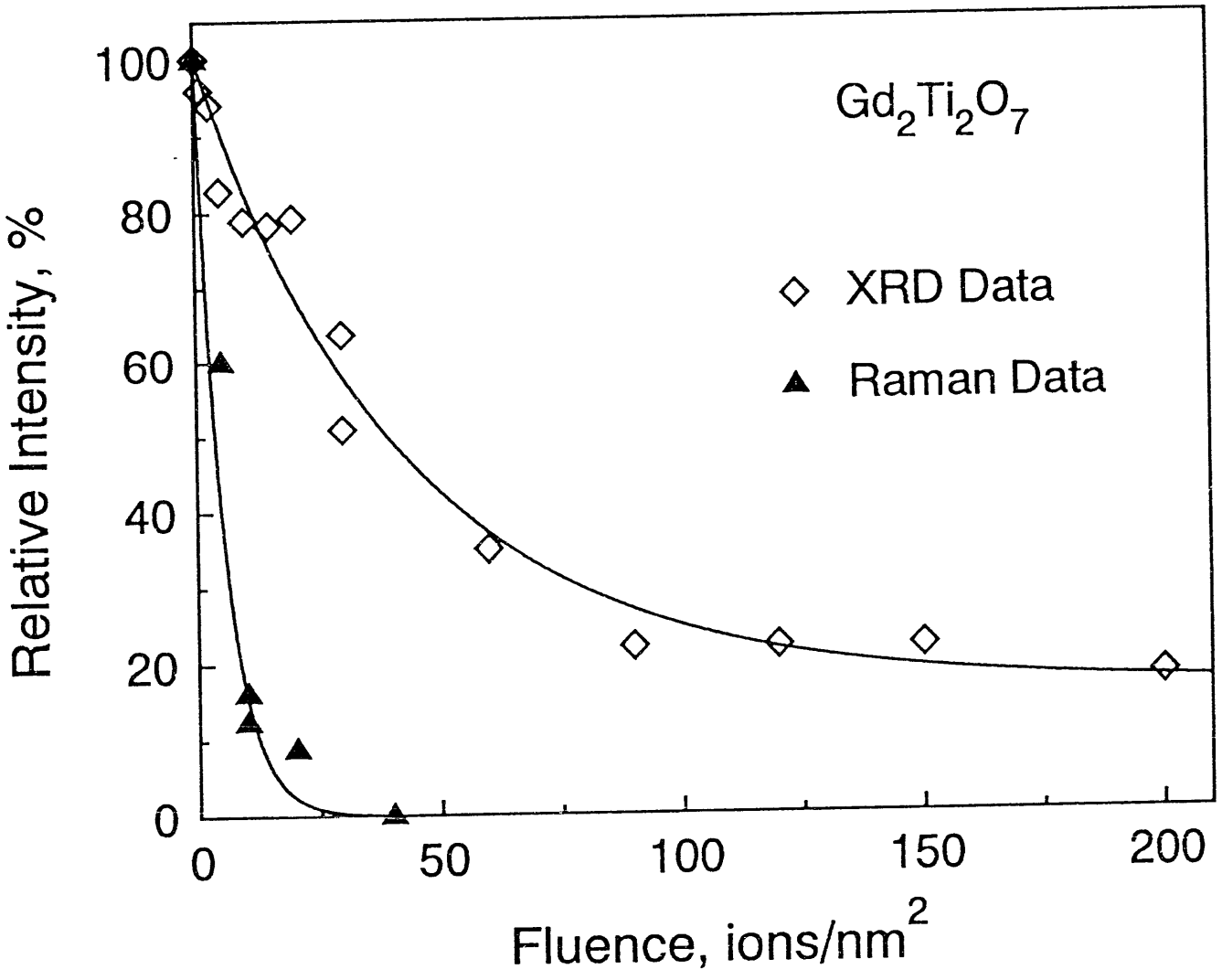
$Gd_2Ti_2O_7$
XRD Data
Raman Data
Relative Intensity, %
100
80
60
40
20
0
0
50
100
150
200
Fluence, ions/nm^2

Fig. 2

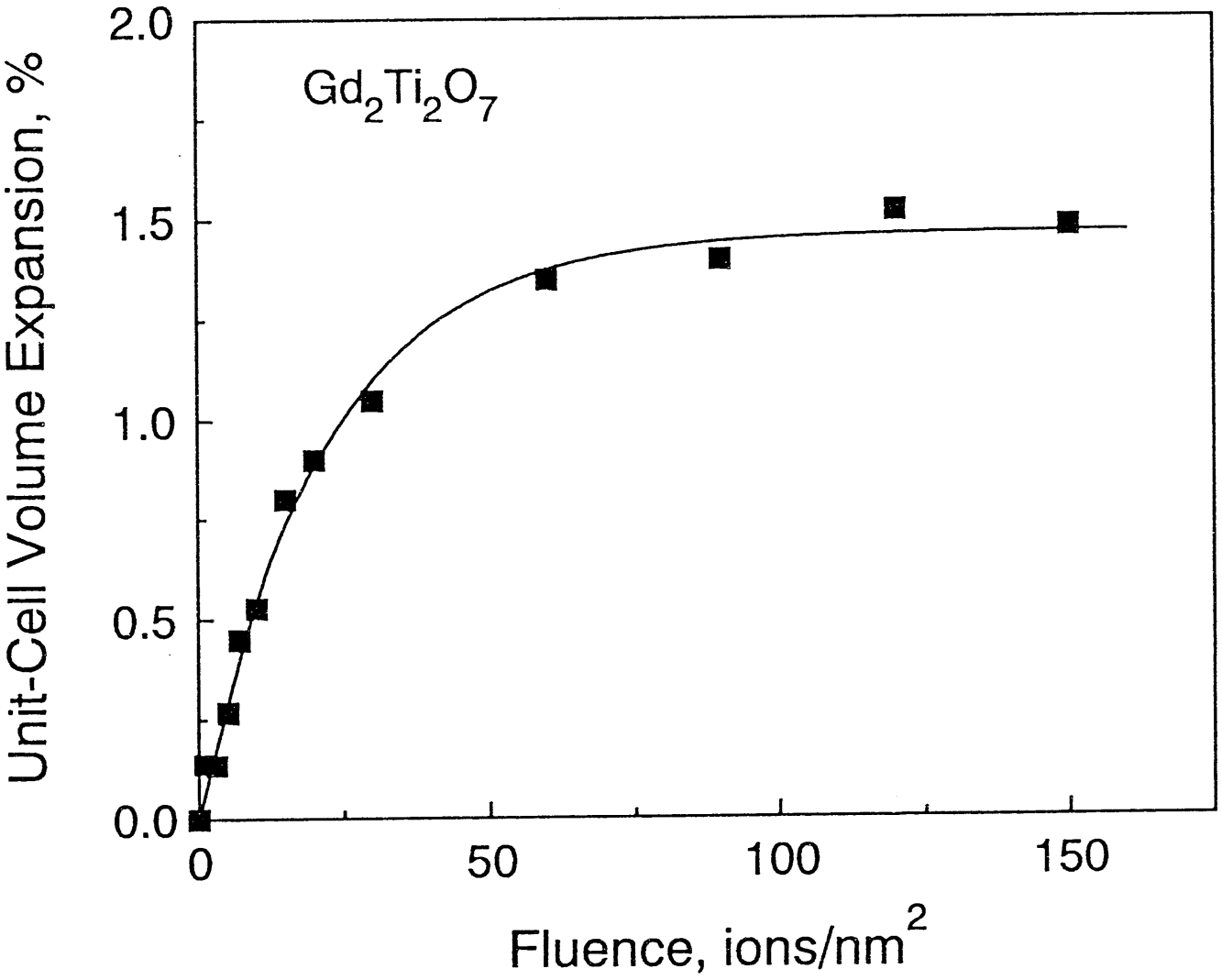
Gd2Ti2O7
Unit-Cell Volume Expansion, %
2.0
1.5
1.0
0.5
0.0
0
50
100
150
Fluence, ions/nm2

Fig. 3

Fig. 4

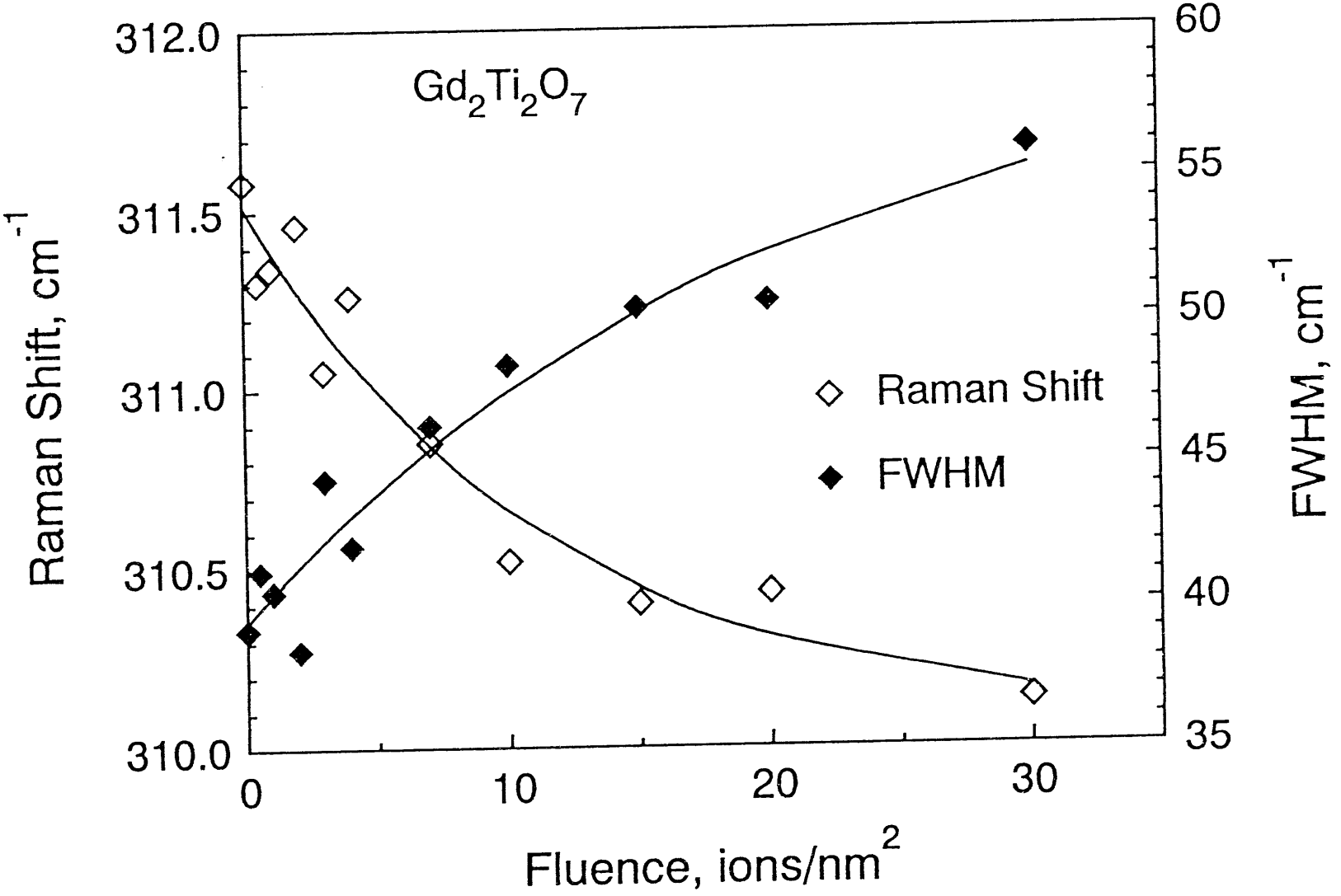
312.0
311.5
311.0
310.5
310.0
0
10
20
30
60
55
50
45
40
35
$Gd_2Ti_2O_7$
Raman Shift
FWHM
Raman Shift, cm^{-1}
FWHM, cm^{-1}
Fluence, $ions/nm^2$

Fig. 5

END

DATE
FILMED
12/24/92